




Research Article

Open Access



Computational design of spatially confined triatomic catalysts for nitrogen reduction reaction

Wei Pei^{1,*,*} , Wenya Zhang^{1,#}, Xueke Yu², Lei Hou¹, Weizhi Xia¹, Zi Wang¹, Yongfeng Liu¹, Si Zhou^{3,*} ,
Yusong Tu^{1,*}, Jijun Zhao² 

¹College of Physics Science and Technology, Yangzhou University, Yangzhou 225009, Jiangsu, China.

²Key Laboratory of Structural Analysis for Industrial Equipment, Dalian University of Technology, Dalian 116024, Liaoning, China.

³School of Physics, South China Normal University, Guangzhou 510631, Guangdong, China.

[#]Authors contributed equally.

* **Correspondence to:** Dr. Wei Pei, Prof. Yusong Tu, College of Physics Science and Technology, Yangzhou University, No.180 Siwangting Road, Yangzhou 225009, Jiangsu, China. E-mail: pwei@yzu.edu.cn; ystu@yzu.edu.cn; Prof. Si Zhou, School of Physics, South China Normal University, No. 378 Huanxi Road, Guangzhou 510631, Guangdong, China. E-mail: sizhou@m.scnu.edu.cn

How to cite this article: Pei W, Zhang W, Yu X, Hou L, Xia W, Wang Z, Liu Y, Zhou S, Tu Y, Zhao J. Computational design of spatially confined triatomic catalysts for nitrogen reduction reaction. *J Mater Inf* 2023;3:26. <https://dx.doi.org/10.20517/jmi.2023.35>

Received: 4 Nov 2023 **First Decision:** 24 Nov 2023 **Revised:** 3 Dec 2023 **Accepted:** 18 Dec 2023 **Published:** 21 Dec 2023

Academic Editors: Fengyu Li, Xingjun Liu **Copy Editor:** Pei-Yun Wang **Production Editor:** Pei-Yun Wang

Abstract

The electrocatalytic process of nitrogen reduction reactions (NRR) offers a promising approach towards achieving sustainable ammonia production, acting as an environmentally friendly replacement for the conventional Haber-Bosch method. Density functional theory calculations have been utilized to design and investigate a set of catalysts known as triple-atom catalysts (TACs) for electrochemical NRR, which are supported on graphite-C₃N₃ nanosheets. Herein, we have systematically evaluated these TACs using stringent screening to assess their catalytic performance. Among the candidates, supported Pt₃, Re₃, and Ru₃ trimers emerged as highly active with decent selectivity, involving a limiting potential range of -0.35--0.11 V. According to analysis of electronic properties, we determined that high NRR activity stems from the *d*- π^* electron-accepting and -donating mechanism. Significantly, the correlation between chemical activity of TACs and electronic structure was established as a pivotal physical parameter, which has led to the conclusion that we can precisely control the catalytic behavior of transition metal trimer clusters by selecting appropriate metal elements and designing moderate cluster-substrates interactions. In summary, these theoretical studies not only enhance our understanding of how catalytic properties are governed by metal-support interactions, regulating stability, activity,



© The Author(s) 2023. **Open Access** This article is licensed under a Creative Commons Attribution 4.0 International License (<https://creativecommons.org/licenses/by/4.0/>), which permits unrestricted use, sharing, adaptation, distribution and reproduction in any medium or format, for any purpose, even commercially, as long as you give appropriate credit to the original author(s) and the source, provide a link to the Creative Commons license, and indicate if changes were made.



and selectivity, but also offer a useful method for screening and designing novel TACs for NRR.

Keywords: Density theory calculation, triple-atom catalysts, nitrogen reduction reaction, metal-support interactions

INTRODUCTION

Ammonia (NH₃) plays a pivotal role as a primary precursor for the production of chemical fertilizers, nitric acid, biofuel energy, plastic, synthetic fiber, *etc.*^[1-4]. Industrially, NH₃ is primarily synthesized through the Haber-Bosch process, involving the reaction of N₂ and H₂ at high temperatures (T > 700 K) and pressure conditions (P > 200 atm)^[5-8]. However, this method consumes a substantial amount of global energy and contributes to significant greenhouse gas emissions^[9,10]. Therefore, it is an urgent need to develop sustainable and clean methods for yielding NH₃ products. Electrochemical nitrogen reduction reactions (NRR) utilizing renewable energy to convert N₂ to NH₃ have recently emerged as a promising alternative^[11-18]. For instance, Geng *et al.* reported the excellent NRR activity of Ru on N-doped carbon, achieving a 29.6% Faradaic efficiency (FE) and an NH₃ production rate of 120.9 μg·mg⁻¹·h⁻¹^[19]. Additionally, the achieved NH₃ yield rate reached 3.665 mg·h⁻¹·mg_{Ru}⁻¹ at a potential of -0.21 V, where the researchers successfully developed a novel approach using N-doped porous carbon (PC) to encapsulate single Ru sites for efficient NRR while maintaining the FE below 9%^[20]. A 5,7-membered carbon ring-involved PC was developed for the electrocatalytic NRR of Ru-embedded PCs by Han *et al.*^[21]. These materials, with an impressive NH₃ yield rate as high as 67.8 ± 4.9 μg·h⁻¹·mg_{cat}⁻¹ and a high FE of 19.5% ± 0.6%, exhibit remarkably favorable catalytic NRR properties as electrocatalysts, surpassing the majority of documented single-atom NRR catalysts. Moreover, theoretical research and calculation models play a key role in predicting highly active and selective catalytic materials^[22], providing important reference values for catalyst preparation. According to density functional theory (DFT) calculations, Azofra *et al.* reported that V₃C₂ possesses the best NRR activity with a 0.64 eV activation barrier among *d*²-*d*⁴ M₃C₂ Mxenes^[23]. Some theoretical work has studied the NRR catalyzed by TM@N₄-G, in which the central transition metal (TM) atom is coordinated by four pyridinic nitrogen atoms. The results show that the limiting potentials of Ti@N₄ (0.69 eV) and V@N₄ (0.87 eV)^[24] are shown to exhibit lower free energy for NRR than that of the Ru(0001) stepped surface (0.98 eV)^[25]. Despite significant progress in this field, many obstacles remain, including high overpotentials (> 0.6 V) and low FEs (9%~29.6%) for NRR. Hence, the development of highly efficient and selective NRR electrocatalysts to facilitate mild condition synthesis of ammonia is crucial.

Over the last few years, the design and synthesis of catalysts have been revolutionized by the advent of atom dispersions^[26,27]. Single-atom catalysts (SACs) have attracted attention for their high-specific activity and maximum metal utilization efficiency^[28-32]. For example, He *et al.* found that a graphdiyne monolayer supported with 11 TM atoms (TM@GDY) exhibits exceptional stability as an electrocatalyst for hydrogen evolution reactions (HER) and oxygen evolution reactions (OER), involving an overpotential range of 0.01~0.46 V^[33]. Moreover, Liu *et al.* conducted research on the electrocatalytic generation of NH₃ from N₂ at room temperature and atmospheric pressure, using nitrogen-doped PC embedded in cobalt, achieving a high ammonia generation rate of 0.86 μmol·cm⁻²·h⁻¹^[34]. Alternatively, other single metal atoms anchored on N-modified carbon-based materials, such as graphitic carbon nitride (g-C₃N₄) and defective graphene, are promising electrocatalysts for NRR with 0.34 V potential^[35]. Despite the potential benefits of SACs, a significant challenge persists in balancing the reaction rate and FE for NH₃ synthesis, mainly due to the involvement of multiple reactive species in the NRR. This challenge remains a major obstacle in the practical application of SACs for the controlled and efficient electrocatalytic generation of NH₃.

Atomic clusters^[36-38], on the other hand, possess unique geometric and electronic properties owing to their strong quantum size effects, rendering them highly promising for catalytic applications. The catalytic activities and product selectivity of supported metal nanoclusters (NCs) were governed with atomic precision by tuning the size and composition of metal NCs. Experimentally, the use of well-dispersed Pt₂ dimers on graphene resulted in a unique catalytic system that significantly increased the aqueous hydrogenation rate of ammonia-borane in comparison to isolated individual Pt-ions. Specifically, the specific rate of the reaction was found to be approximately 17 times higher when using the Pt₂ dimers^[39]. Furthermore, a Mo₃ trimer on graphdiyne nanosheets was observed to exhibit the highest activity, selectivity, and stability towards NRR based on the designed screening criteria, involving a calculated initial voltage of -0.32 V^[40]. More importantly, the presence of several active sites in a catalyst is essential to broaden the range of adsorbate binding capabilities and to facilitate the catalysis of a broader spectrum of complex reactions to yield diverse products. Tian *et al.* fabricated diatomic Fe₂ NCs anchored on mesoporous carbon nitride, which demonstrated remarkable catalytic activity in the conversion of stilbene to oxide, achieving a high selection of 93% while maintaining a transformation rate of 91%^[41]. Ru₃ stabilized on nitrogen-doped carbon nanosheets was reported to efficiently catalyze the selective oxidation of alcohols^[42]. Moreover, theoretical studies have suggested that supported metal NCs exhibit remarkable abilities in catalyzing reactions involving the activation of inert reactant molecules or requiring multiple reaction centers^[43-47]. For example, a tetramer immobilized in nitrogen-doped graphene monolayers shows optimal surface activities for N₂ activation and subsequent reaction to yielding NH₃ products, involving the calculational on-set potential of -0.45 V, significantly lower than that of supported single atoms and dimers^[47]. Li *et al.* discovered that Rh₃-C₂N exhibited superior catalytic performance in the enzymatic pathway with a limiting voltage of only -0.45 V compared to Rh₁-C₂N and Rh₂-C₂N^[48]. Furthermore, Zheng *et al.* have designed a set of electrocatalysts known as triple-atom catalysts (TACs). The theoretical insights suggest that the Co₃-N₄ system has a superior catalytic activity, attaining a boundary potential of -0.41 V via the enzymatic mechanism for NRR^[46].

Motivated by the substantial progress in both experimental and theoretical studies, we have systematically investigated the stability of 3d-5d TM trimers embedded on C₃N₃ nanosheets (marked as TM₃@C₃N₃) using DFT calculations and evaluated their electrocatalytic performances for NRR. The theoretical results indicate that TM₃@C₃N₃ (TM = Re, Ru, Pt) holds significant promise electrocatalysts for the NRR, demonstrating excellent performance and feasibility. Significantly, the Re₃@C₃N₃ system demonstrates exceptional catalytic activity, surpassing other catalysts, with a limiting potential of -0.11 V using the consecutive mechanism. Furthermore, we established a correlation between the inherent electronic characteristics of TM₃@C₃N₃ and its catalytic performance, identifying significant physical parameters. Additionally, we advocate the concept of designing TACs as a strategic approach to drive the development of advanced electrocatalysts within the framework of green hydrogen economics.

MATERIALS AND METHODS

The Vienna *ab initio* simulation package (VASP) was utilized to conduct spin-polarized DFT computations, employing the plane wave basis set^[49,50]. We employed projector augmented wave (PAW) potentials along with an energy cutoff of 500 eV^[51,52]. The Perdew-Burke-Ernzerhof (PBE) functional of generalized gradient approximation (GGA) was employed as the exchange-correlation functional^[53]. It has been extensively tested and successfully applied to an array of solid-state and molecular systems^[22-26,54]. The van der Waals (vdW) interaction was investigated using Grimme's semiempirical DFT-D3 scheme with dispersion correction^[55,56]. The energy and force convergence thresholds were established at 10⁻⁴ eV and 0.02 eV·Å⁻¹, correspondingly. To avoid any interaction between two periodic units, a (2 × 2) supercell of C₃N₃ monolayer with a 16 Å vacuum space along the z-direction was employed. Moreover, the Brillouin zone was sampled at

the k -point using a $2 \times 2 \times 1$ grid^[57]. *Ab initio* molecular dynamics (AIMD) simulations were performed at a temperature of 300 K in an NVT ensemble for a duration of 10 ps in order to estimate the thermodynamic stability of the $\text{TM}_3@C_3N_3$ systems.

The binding energies (E_b) were calculated to judge the thermodynamic stabilities of the designed $\text{TM}_3@C_3N_3$ systems, as follows:

$$E_b = E_{\text{TM}_3@C_3N_3} - E_{C_3N_3} - E_{\text{TM}_3} \quad (1)$$

where $E_{\text{TM}_3@C_3N_3}$, $E_{C_3N_3}$, and E_{TM_3} denote the total energy of C_3N_3 substrate anchored with transition-metal trimeric clusters, the optimized pristine C_3N_3 , and the isolated transition-metal trimeric clusters, respectively. The electronic adsorption energy (E_{ads}) of reaction intermediates on $\text{TM}_3@C_3N_3$ substrates can be computed by the following formula:

$$E_{\text{ads}} = E_{\text{tot}} - E_{\text{cat}} - E_{\text{adsorbate}} \quad (2)$$

where E_{tot} is the total energy of $\text{TM}_3@C_3N_3$ substrates adsorbed by the intermediate, and E_{cat} and $E_{\text{adsorbate}}$ are the energy of $\text{TM}_3@C_3N_3$ and the adsorbed intermediate, respectively. According to the proposal by Nørskov *et al.*^[58-60], the calculated hydrogen electrode (CHE) model can be employed to determine the Gibbs free energy change (ΔG) for each individual step in the electrochemical hydrogenation process, and the ΔG value is calculated by employing the formula as follows:

$$\Delta G = \Delta E + \Delta E_{\text{ZPE}} - T\Delta S + \Delta G_U + \Delta G_{\text{pH}} \quad (3)$$

where ΔE is the total reaction energy gained from the DFT calculations. ΔE_{ZPE} and ΔS are the changes in zero-point energy and entropy, respectively. The zero-point energy and entropy were determined by calculating the vibrational frequencies. The temperature (T) was set to 298.15 K in this research. ΔG_U denotes the impact of the applied potential (U) and is equal to $-neU$, where n corresponds to the number of electrons transferred. The correction of pH, ΔG_{pH} , represents the free energy and can be calculated according to the formula: $\Delta G_{\text{pH}} = -K_B T \times \text{pH} \times \ln 10$. The pH value is assumed to be 0, and K_B refers to the Boltzmann constant. The quantities of transferred electrons and the potential of the applied electrode are represented by e and U , respectively. The potential determination step (PDS), which has the maximum ΔG value, can be used to determine the limiting potential (U_{limiting}) of the entire reduction process in an acid solution using the following formula:

$$U_{\text{limiting}} = -\Delta G_{\text{max}}/e \quad (4)$$

RESULTS AND DISCUSSION

Geometry and stability of $\text{TM}_3@C_3N_3$

Since the NRR is a complex process including various reactive species, the use of effective screening descriptors is crucial. As illustrated in [Figure 1](#), we propose a standard strategy for screening candidate catalysts for N_2 reduction reaction. (1) Thermodynamic stability: TACs should have thermodynamics ($\Delta E_b < 0$ eV, where ΔE_b is the binding energy of TM_3 atoms on C_3N_3). Additionally, their dynamic stability should be confirmed through AIMD simulations at 300 K, ensuring that the structure remains stable without deformation; (2) Surficial activity: N_2 should undergo complete activation ($\Delta G_{-N_2} < 0.50$ eV, indicating chemical adsorption of N_2 , where the asterisk * denotes the adsorption site)^[61]; (3) Energy cost: the potential range of NRR reaction on Ru-based catalysts with high catalytic performance under mild conditions is

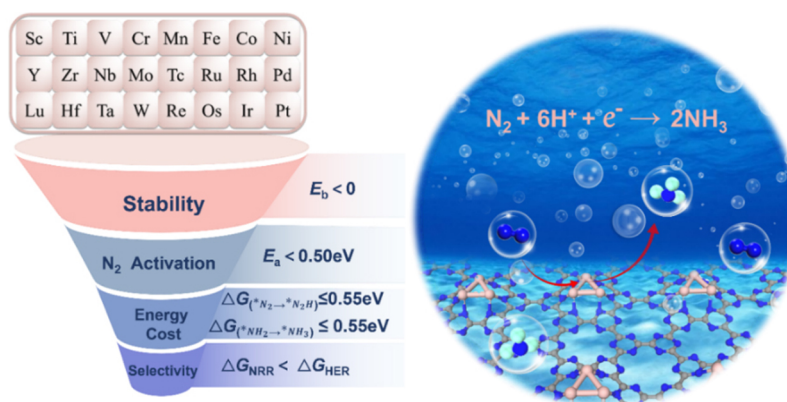


Figure 1. The schematic diagram for screening candidate TACs for NRR. HER: Hydrogen evolution reactions; NRR: nitrogen reduction reactions; TACs: triple-atom catalysts.

-0.50~-0.56 V. Therefore, in this paper, catalytic properties of NRR: the limit potential, U_{limiting} , is used to evaluate NRR activity. To ensure low energy costs, we use a standard of 0.55 eV. For the first and last hydrogenation steps, which are typically the most likely limiting steps in a reaction, it is desirable to have ΔG values that are as low as possible ($\Delta G_{\text{N}_2 \rightarrow \text{NNH}} \leq 0.55 \text{ eV}$ and $\Delta G_{\text{NH}_2 \rightarrow \text{NH}_3} \leq 0.55 \text{ eV}$)^[61,62]. The calculation of ΔG is performed using Equation (3)^[61]; (4) NRR vs. HER selectivity: to ensure high NRR selectivity, the Gibbs free energy value of hydrogen adsorption should exceed that of nitrogen. These criteria collectively form a robust filtration strategy for identifying potential NRR catalysts.

Next, we first consider the stability of the metal trimer on C_3N_3 before delving into the electroreduction process. Through extensive geometric optimization and configuration search, we obtained the structures of $\text{TM}_3@C_3N_3$. As summarized in Figure 2A, these metal trimer clusters show the strong binding strength on the C_3N_3 monolayer, involving E_b of -9.57~-4.22 eV, which indicates decent thermodynamic stabilities. The E_b is calculated by Equation (1) with the detailed data shown in Table 1. Furthermore, according to the above calculation, it is worth noting that $\text{Pd}_3@C_3N_3$ possesses the weakest binding strength among the 21 selected systems. In light of this, we conducted AIMD at 300 K for 10 ps to evaluate the stability of $\text{TM}_3@C_3N_3$, with $\text{Pd}_3@C_3N_3$ considered as a representative. Figure 2B and C illustrates the oscillations of the DFT total energies (E) relative to the initial conditions and temperature (T), along with the $d_{\text{Pd-N}}$ and $d_{\text{Pd-Pd}}$, indicating dynamic fluctuations near the initial condition. According to the captured structures of $\text{Pd}_3@C_3N_3$ under different times [Figure 2D], it is preserved well and maintains structural stability, in which the vertical buckling exhibits minimal fluctuation, measuring less than 0.10 Å. Therefore, combined with the above calculations, we can confidently assert that these $\text{TM}_3@C_3N_3$ systems have robust structural stabilities.

Activation of N_2 on $\text{TM}_3@C_3N_3$

In the overall electrochemical NRR process, the primary and critical step involves the adsorption and activation of N_2 molecules, a process of utmost importance as it is responsible for activating the $\text{N}\equiv\text{N}$ triple bond, laying the foundation for the smooth protonation to follow. Figure 3A shows that the activation of N_2 is facilitated via an electron transfer mechanism, where the partially filled d orbitals of TM atoms accept electrons from N_2 molecules while simultaneously donating d electrons to the anti-bonding orbitals (π^*) of $^*\text{N}_2$ in the reverse direction. Therefore, this interaction strengthens the TM-N bond while attenuating $\text{N}\equiv\text{N}$. Notably, the metal double or triple-atom centers are critical to maximizing the activation effect by donating a greater number of electrons to N_2 in comparison to monatomic active sites^[63-66]. Using dual-metal or triple-atom centers proves to be a more effective approach in promoting N_2 activation. Employing this approach provides an advantage in surmounting the barrier encountered during the initial step in the

Table 1. DFT-calculated the average distances of TM-N ($d_{\text{TM-N}}$) and TM-TM ($d_{\text{TM-TM}}$), vertical buckling between TM_3 and C_3N_3 monolayer ($d_{\text{TM-C}}$), combining energy (ΔE_{bind}), d orbital centroid (ϵ_d), magnetic moment (Mag), and the number of CT between TM_3 and C_3N_3 monolayers

System	$d_{\text{TM-N}}$ (Å)	$d_{\text{TM-TM}}$ (Å)	$h_{\text{TM-C}}$ (Å)	ΔE_{bind} (eV)	ϵ_d (eV)	Mag (μB)	CT (e)
Ti	2.01	2.52	1.27	-9.14	0.72	3.23	1.60
V	2.03	2.38	1.53	-9.01	0.46	0.00	0.58
Cr	1.94	1.93	0.89	-8.63	-0.56	0.00	0.24
Mn	1.97	2.33	0.97	-7.44	-1.49	4.96	0.60
Fe	1.92	2.27	1.47	-6.98	-1.93	6.16	0.33
Co	1.88	2.22	1.23	-7.35	-1.53	3.00	0.47
Ni	1.86	2.21	1.17	-7.47	-1.58	0.00	0.46
Y	2.18	3.53	2.01	-9.48	1.87	0.99	1.27
Zr	2.09	3.00	1.37	-9.46	0.77	1.92	1.97
Nb	2.07	2.59	1.31	-7.95	0.77	0.77	1.63
Mo	2.09	2.19	1.23	-7.51	-0.92	0.61	0.38
Ru	2.03	2.51	1.73	-7.38	-1.59	0.00	0.30
Rh	2.07	2.55	1.50	-6.46	-1.75	0.71	0.35
Pd	2.11	2.59	1.37	-4.22	-2.09	0.00	0.24
Hf	2.89	2.10	1.41	-9.57	1.01	1.24	1.85
Ta	2.55	2.10	1.28	-9.07	0.39	0.07	1.00
W	2.45	2.08	1.17	-6.59	-0.35	0.11	0.88
Re	2.35	1.99	1.06	-9.13	-1.01	0.96	0.65
Os	2.43	2.06	1.20	-8.18	-1.41	0.00	0.47
Ir	2.42	2.02	0.68	-7.70	-2.02	0.00	0.40
Pt	2.51	2.21	1.77	-5.25	-2.53	0.02	0.26

CT: Charge transfers; DFT: density functional theory; TM: transition metal.

hydrogenation of NRR. By incorporating multiple metal atoms in the catalytic centers, the activation of N_2 becomes more efficient, enhancing the overall performance of the NRR process.

Revealing the source of NRR activity in electrocatalysts provides guidance for designing and developing highly active catalysts. To uncover the fundamental mechanism behind the activation of N_2 , we employed the PBE functional to calculate the partial density of states (PDOS), enabling us to gain deeper insights into the nature of the interactions and the extent of N_2 activation facilitated by the metal trimers^[67,68]. The enhanced ability of $\text{Pt}_3/\text{g-C}_3\text{N}_3$ to adsorb and activate N_2 , as compared to the free N_2 , can be attributed primarily to the presence of vacant and filled d orbitals. As displayed in Figure 3B, the empty $5d$ orbitals of Pt_3 receive electrons from N_2 , resulting in the formation of bonding states. Simultaneously, a robust $d-2\pi^*$ orbital coupling takes place, causing the $2\pi^*$ orbital from N_2 to be fractionally filled in the vicinity of the Fermi level. The partial filling is accomplished by the electron feedback from the occupied d orbitals of Pt_3 to the $2\pi^*$ orbital of N_2 . The observed outcome provides additional evidence to support the presence of strong $d-\pi^*$ orbital coupling in close proximity to the Fermi level. Additionally, it affirms the significant overlap between the d orbitals of trimeric clusters and the filled orbitals of adsorbed N_2 . This finding strongly aligns with the earlier analysis and supports the proposed mechanism of N_2 activation.

To further understand the interacting nature of N_2 and $\text{TM}_3@\text{C}_3\text{N}_3$ catalysts, we conducted calculations to determine the $\Delta G_{\text{N}_2^*}$ value. The corresponding adsorption free energy for N_2 adsorption on $\text{TM}_3@\text{C}_3\text{N}_3$ is calculated by Equation (3), with the detailed data presented in Figure 3C and Supplementary Table 1, respectively. It is not difficult to see that for most $\text{TM}_3@\text{C}_3\text{N}_3$ catalysts, the $\Delta G_{\text{N}_2^*}$ value is close to the zero,

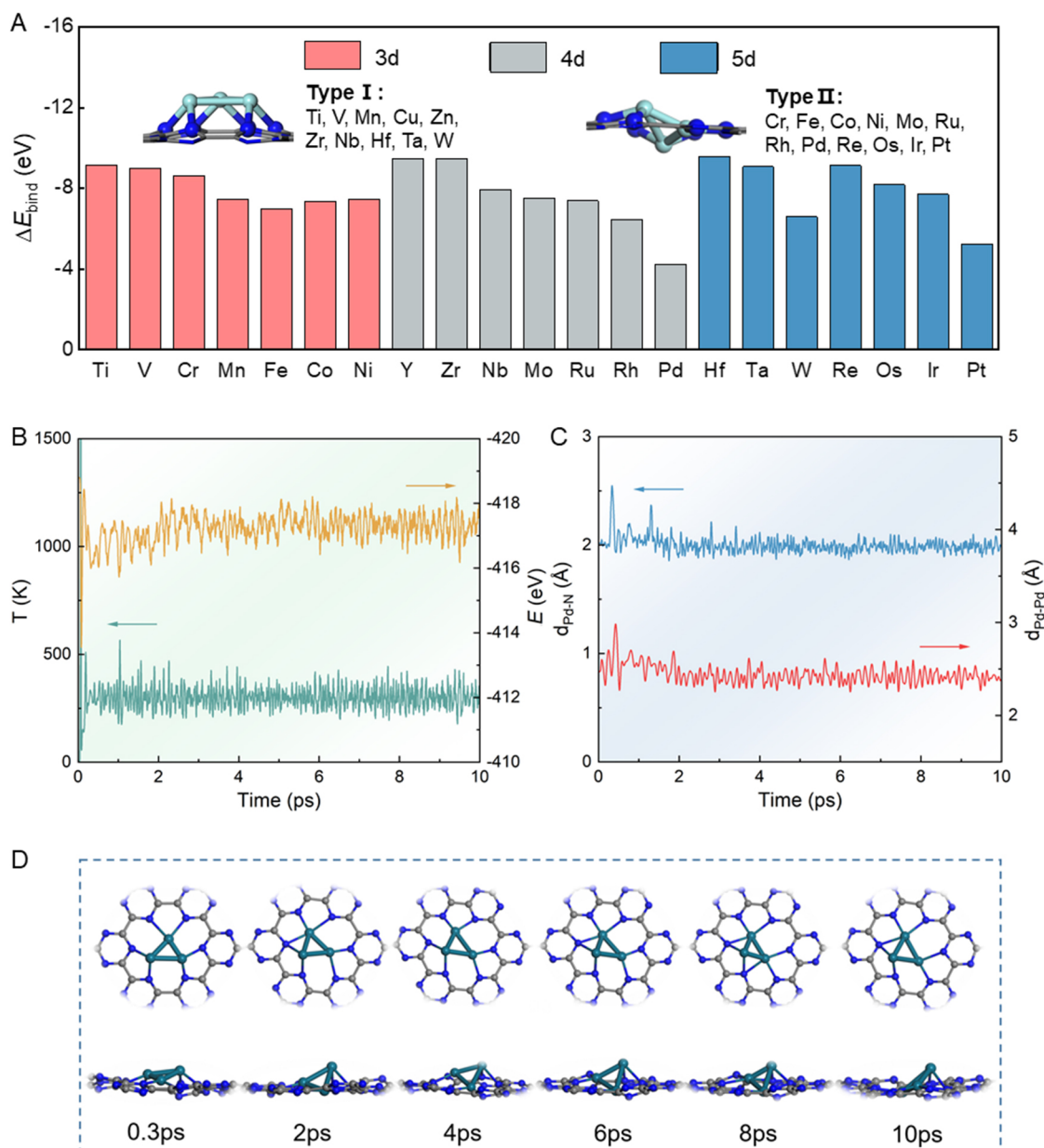


Figure 2. (A) Computed the binding energies (ΔE_{bind}) of triple-atoms anchored on C_3N_3 . The grey, blue, and light green are C, N, and metal atoms, respectively; (B) Variations of the temperature (T) and total energies (E); and (C) the distances of Pd-N ($d_{\text{Pd-N}}$) and Pd-Pd ($d_{\text{Pd-Pd}}$) vs. time for AIMD simulations of $\text{Pd}_3@C_3N_3$; (D) $\text{Pd}_3@C_3N_3$ structures are captured within 10 ps, with the Pd shown in green. AIMD: *Ab initio* molecular dynamics.

ranging from 0.35 to -5.12 eV, implying that the N_2 molecule exhibits favorable adsorption characteristics on these catalysts. In comparison to the original $\text{N}\equiv\text{N}$ triple bond length in N_2 molecules [Table 1], regardless of whether the N_2 molecule is adsorbed in an end-on or side-on configuration, a noticeable elongation is observed in the $\text{N}\equiv\text{N}$ triple bond, indicating that the adsorption of N_2 on the selected 21 catalysts can attenuate the $\text{N}\equiv\text{N}$, facilitating the activation of the subsequent NRR process. According to Bader charge analysis, Figure 3D and E shows that the TM atoms and N atoms are indicated to undergo a significant charge transfer, and the metal trimer cluster loses an electron ranging from 0.24 to 1.97 e [Table 1]. As shown in Figure 3F, the adsorption energy of N_2 is linearly related to the d -orbital center (ϵ_d) of

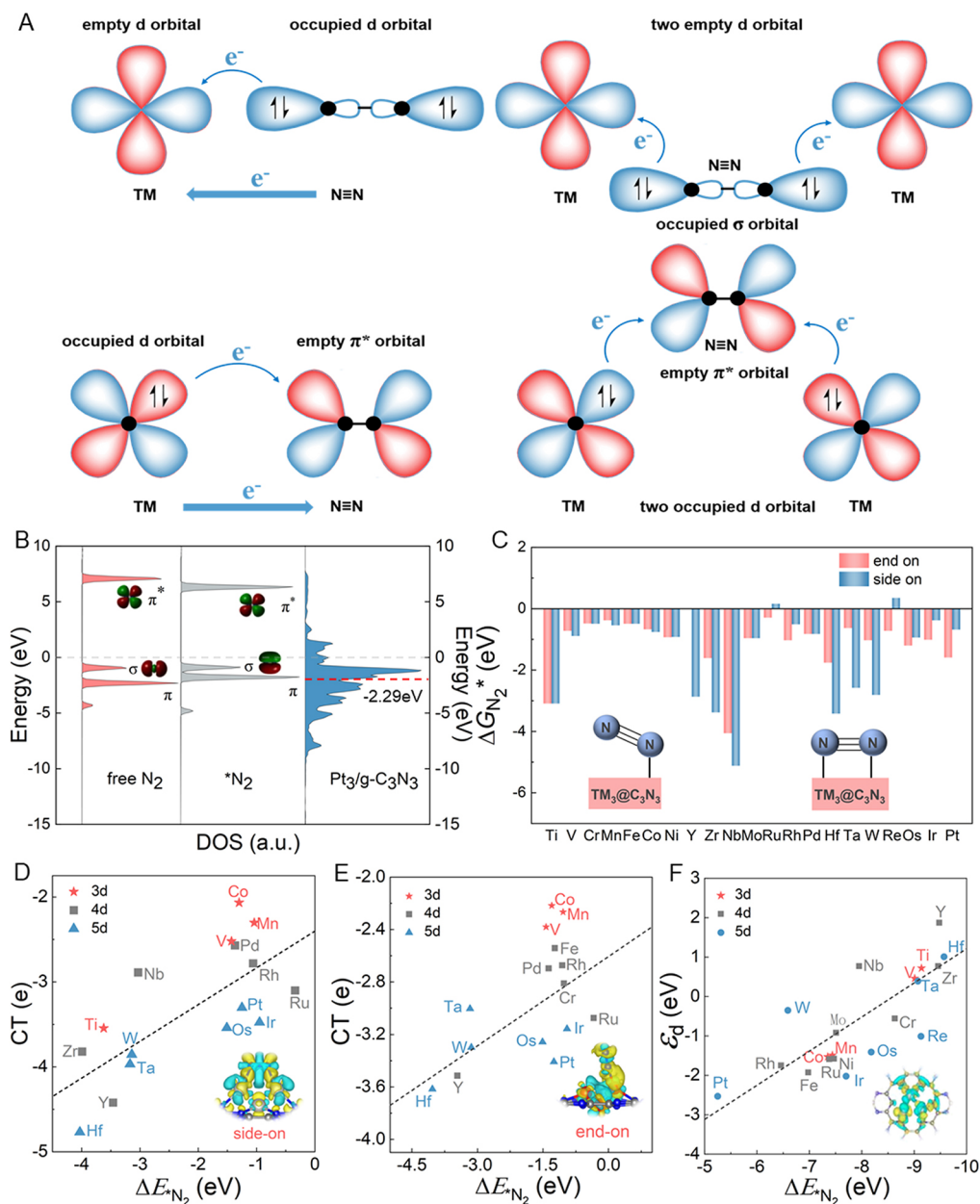


Figure 3. (A) Simplified schematic illustration of N_2 binding to single- and double-atom sites; (B) Computed molecular orbitals showing the electronic structure of free N_2 and N_2 adsorbed on $Pt_3/g-C_3N_3$. The red dashed line is the d -band center; (C) The adsorption free energies (ΔG_{N_2}) of N_2 on $TM_3@C_3N_3$. The number of CT of N_2 with (D) side-on and (E) end-on configurations vs. its adsorption energies (ΔE_{N_2}); (F) The d -orbital center (ϵ_d) of $TM_3@C_3N_3$ vs. ΔE_{N_2} . The inset is the differential charge density of N_2 on $TM_3@C_3N_3$ and $TM_3@C_3N_3$. CT: Charge transfers; DOS: density of states; TM: transition metal.

the metal clusters. The higher the d orbital center of the $TM_3@C_3N_3$ system, the more favorable its interaction with the π^* orbital of N_2 and provides more charge transfer to the N_2 molecule, thus showing a stronger binding capacity for N_2 adsorption^[69-72]. Guided by these essential parameters, the catalytic response of TM trimer clusters can be finely regulated and manipulated by designing moderate cluster-carrier interactions through the selection of suitable metal elements.

Reaction mechanism of electrochemical NRR

As shown in [Figure 4A](#), one reaction mechanism for the electrocatalytic synthesis of ammonia, namely the enzymatic mechanism, is depicted, and an additional consecutive mechanism is presented in [Supplementary Figure 1A](#). The distal mechanism and the alternative mechanism are also detailed in [Supplementary Figure 1B](#). A common feature among them is that the N atom at one end of N_2 is adsorbed on the catalyst, while the N element at the other end is not adsorbed. However, the N element at the far end preferentially reacts with the H proton. In the distal mechanism, N atoms leaving the surface of the catalyst preferentially react with H protons and release as ammonia, leaving $*N$ adsorbed on the catalyst, which will start hydrogenation and form ammonia. An alternative mechanism involves hydrogenating two N atoms using six proton-electron pairs to form two NH_3 molecules. Contrarily, in the enzymatic pathway, the N_2 molecule is first decomposed into adsorbed $*N$ atoms, and then, $*N$ is gradually hydrogenated into ammonia. The hydrogenation process follows the same pathway as the alternative mechanism. In the consecutive mechanism, one of the N atoms undergoes hydrogenation first and subsequently reacts with the remaining N atoms, resulting in the formation of the second NH_3 molecule. Owing to the distinct structures and performances of catalysts, the NRR reaction mechanism often varies. Nevertheless, numerous studies have shown that the initial or final step can be considered the potential determinant independent of NRR mechanisms^[73-75]. The proton step with the maximal positive free energy change (ΔG_{\max}) is defined as the PDS. It is well known that the ideal catalyst for an electrochemical NRR should meet the following criteria: (1) The ΔG_{\max} of the two key steps is below 0.55 eV, that is, $\Delta G_{N_2 \rightarrow *NNH} \leq 0.55$ eV and $\Delta G_{*NH_2 \rightarrow *NH_3} \leq 0.55$ eV, so the performance of the catalyst in question is superior to that of the best pure metal or nanometal cluster catalyst; (2) $E_{\text{ads}(*N_2)} - E_{\text{ads}(*H)} < 0$, which proves that N_2 has good selectivity in catalysts.

For a prompt evaluation of $TM_3@C_3N_3$ catalysts regarding their NRR performance, we calculated the ΔG for the initial and final stages of NRR under open-circuit conditions ($U = 0$). The resulting values, along with corresponding diagrams, are presented in [Table 2](#) and [Supplementary Figure 2](#). Four classifications are considered to evaluate the critical steps, with the critical point set at 0.55 eV. Consequently, six systems met the above criteria, demonstrating decent catalytic activity in electrochemical NRR. In the case of $Pt_3@C_3N_3$, the associated free energy diagram is presented in [Figure 4B](#). The $Pt_3@C_3N_3$ exhibits a propensity for NRR via enzymatic mechanisms, wherein N_2 adopts a side-on configuration. In the enzymatic mechanism, the initial step of hydrogenation involves the formation of a chemical bond between a hydrogen atom and one of the N atoms, followed by alternating bonding to the two N atoms until a second NH_3 molecule is produced. The ΔG_{\max} change is 0.24 eV, establishing the final hydrogenation step as the PDS of the entire electrochemical NRR. Similarly, we investigated the NRR pathway on $Ru_3@C_3N_3$, as depicted in [Figure 4C](#), revealing a ΔG_{\max} of 0.35 eV.

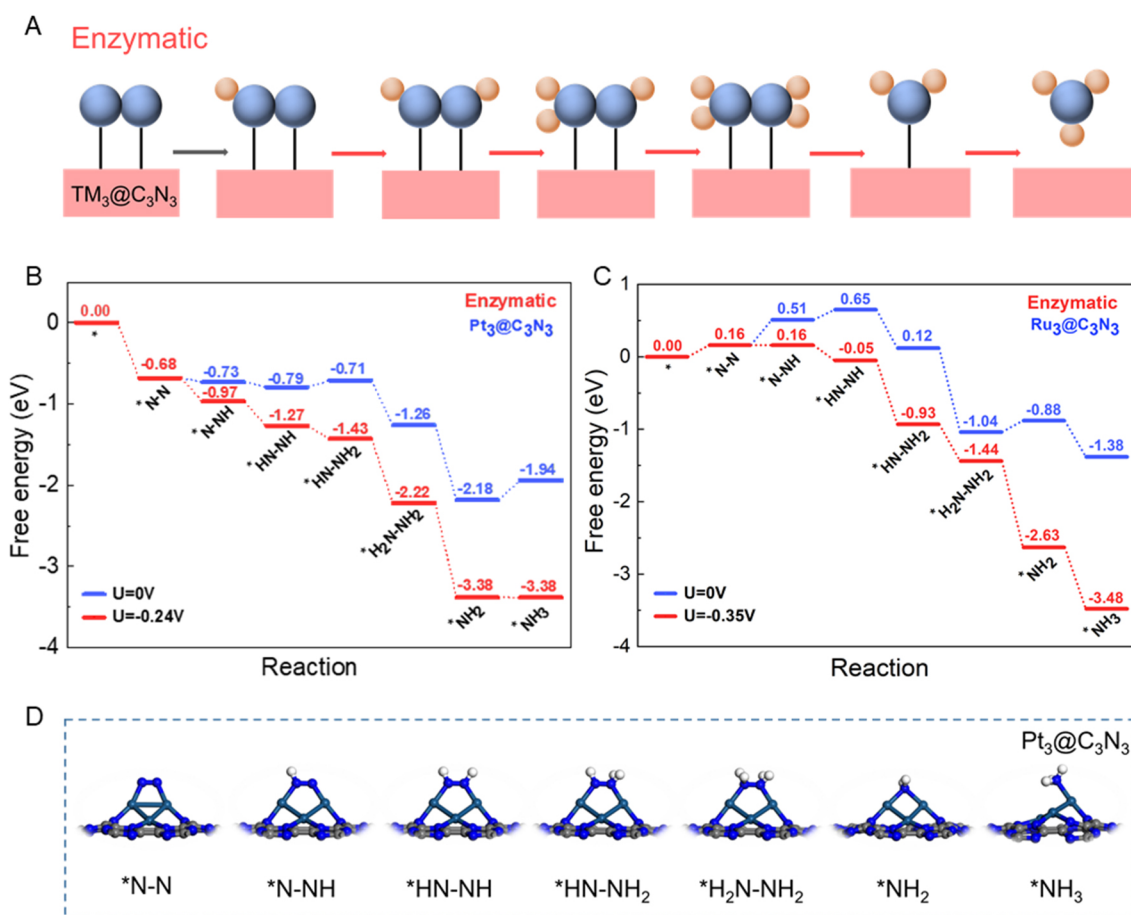
The relevant intermediate geometries of $Pt_3@C_3N_3$ for each step are presented clearly in [Figure 4D](#). It is evident that throughout the entire NRR process, the initial step ($*N_2 \rightarrow *NNH$) is identified as the PDS. Briefly speaking, for $Pt_3@C_3N_3$ catalysts, the corresponding limiting potential (U_L) value is -0.24 V, while for $Ru_3@C_3N_3$ catalysts, the U_L value is -0.35 V. Consequently, by applying the U_L to the surfaces of $Pt_3@C_3N_3$ and $Ru_3@C_3N_3$ catalysts, it is ensured that all electron transfer steps occur spontaneously without any uphill energy barriers, which is beneficial to the production of NH_3 , where the reaction process of $Ru_3@C_3N_3$ also follows an enzymatic mechanism.

It is worth emphasizing that the development of efficient NRR catalysts remains challenging due to the competition with HER^[66,76,77]. An ideal NRR catalyst would demonstrate significantly higher NRR activity and considerably lower HER activity. To assess selectivity, we calculated the N_2 adsorption energy and hydrogen adsorption energy on the designed $TM_3@C_3N_3$ catalysts using Equation (2). A more negative difference between N_2 adsorption energy and hydrogen adsorption energy indicates higher selectivity for

Table 2. DFT-calculated potential-determining steps (including reaction mechanisms and corresponding reactions) and corresponding limiting potentials (U_L) for $TM_3@C_3N_3$ (TM = Re, Pt, Ru, Rh, Ta, Ir)

$TM_3@C_3N_3$	Potential-determining step		U_L (V)
	Mechanism	Reaction	
Re	Consecutive	$*HNNH + H^+ + e^- \rightarrow *HNNH_2$	-0.11
Pt	Enzymatic	$*NH_2 + H^+ + e^- \rightarrow *NH_3$	-0.24
Ru	Enzymatic	$*N_2 + H^+ + e^- \rightarrow *NNH$	-0.35
	Consecutive	$*NNH + H^+ + e^- \rightarrow *NNH_2$	-0.40
Rh	Enzymatic	$*N_2 + H^+ + e^- \rightarrow *NNH$	-0.40
	Consecutive		
Ta	Consecutive	$*HNNH + H^+ + e^- \rightarrow *HNNH_2$	-0.42
Ir	Enzymatic	$*NH_2 + H^+ + e^- \rightarrow *NH_3$	-0.54
	Consecutive		

DFT: Density functional theory; TM: transition metal.

**Figure 4.** (A) Schematic illustration of Enzymatic mechanism towards NH_3 formation on $TM_3@C_3N_3$. Diagrams for N_2 electroreduction via enzymatic mechanism on (B) $Pt_3@C_3N_3$ and (C) $Ru_3@C_3N_3$; (D) The optimized geometry of various intermediates on the $Pt_3@C_3N_3$ structure along the enzymatic pathway of NRR. NRR: Nitrogen reduction reactions.

NRR. The results are presented in [Supplementary Figure 3](#). It is evident that both $Pt_3@C_3N_3$ and $Ru_3@C_3N_3$, which were previously identified as having the highest NRR activity, exhibit markedly higher selectivity for NRR over HER. These findings imply that these catalysts can ensure a high Faraday efficiency in catalytic electrochemical NRR.

CONCLUSIONS

In summary, this study provides a systematic investigation into the potential of C_3N_3 -loaded TACs in electrocatalytic NRR using DFT calculations. Employing a stringent “five-step” filtering strategy, we have identified $TM_3@C_3N_3$ ($TM = Pt, Ru, Re$) as highly promising candidates with the attributes of low energy cost, high selectivity, remarkable stability (both thermodynamic and kinetic), and remarkably low limiting potentials ($-0.35 \sim -0.11$ V). Our analysis of electronic properties highlights that the exceptional NRR activity can be ascribed to the electron acceptance and donation mechanism involving $d-\pi^*$ interactions. This mechanism, combined with charge density differences and PDOS, underscores the qualifications of $TM_3@C_3N_3$ as electrocatalysts. Furthermore, we have explored the linkage between chemical activity and the electronic structure of $TM_3@C_3N_3$ surfaces, revealing a pivotal physical parameter that allows precise control over the catalytic performance of TM trimer clusters. In conclusion, this work significantly improves our overall comprehension regarding the stability, activity, and selectivity of $TM_3@C_3N_3$ electrocatalysts. Moreover, it provides a valuable methodology for efficiently screening and designing innovative TACs specifically tailored for NRR. We anticipate that these findings will ignite further exploration and experimentation, both in theory and practice, aiming to unlock the vast potential of TACs in NRR and its associated electrochemical reactions.

DECLARATIONS

Authors' contributions

Made substantial contributions to the conception and design of this article, writing, and editing: Pei W, Zhang W, Yu X

Made substantial contributions to the collation of literature and writing: Liu Y, Zhou S, Tu Y, Zhao J

Performed data analysis and discussion: Hou L, Xia W, Wang Z

Availability of data and materials

[Supplementary materials](#) are available from the Journal of Materials Informatics or from the authors.

Financial support and sponsorship

This work was supported by the National Natural Science Foundation of China (Nos. 12304300, 11974068, 91961204, and 12075201), the Natural Science Foundation of Jiangsu Province (Nos. BK20230555 and BK20230563), the Natural Science Foundation of Jiangsu Higher Education Institutions of China (No. 23KJB140019), the Fundamental Research Funds for the Central Universities of China (Nos. DUT20LAB110 and DUT22ZD103), Outstanding Doctor Program of Yangzhou City “Lv Yang Jin Feng” (No. YZLYJFJH2022YXBSO84), and Open Research Fund of CNMGE Platform & NSCC-TJ (CNMGE2023007). The authors acknowledge the computer resources provided by the Shanghai Supercomputer Center.

Conflicts of interest

All authors declared that there are no conflicts of interest.

Ethical approval and consent to participate

Not applicable.

Consent for publication

Not applicable.

Copyright

© The Author(s) 2023.

REFERENCES

1. Galloway JN, Townsend AR, Erismann JW, et al. Transformation of the nitrogen cycle: recent trends, questions, and potential solutions. *Science* 2008;320:889-92. DOI
2. Klerke A, Christensen CH, Nørskov JK, Vegge T. Ammonia for hydrogen storage: challenges and opportunities. *J Mater Chem* 2008;18:2304-10. DOI
3. Guo J, Chen P. Catalyst: NH₃ as an energy carrier. *Chem* 2017;3:709-12. DOI
4. Gao S, Liu X, Wang Z, et al. Spin regulation for efficient electrocatalytic N₂ reduction over diatomic Fe-Mo catalyst. *J Colloid Interface Sci* 2023;630:215-23. DOI
5. Zhang G, Zhang X, Meng Y, Pan G, Ni Z, Xia S. Layered double hydroxides-based photocatalysts and visible-light driven photodegradation of organic pollutants: a review. *Chem Eng J* 2020;392:123684. DOI
6. Chen JG, Crooks RM, Seefeldt LC, et al. Beyond fossil fuel-driven nitrogen transformations. *Science* 2018;360:eaar6611. DOI PubMed PMC
7. Yang X, Nash J, Anibal J, et al. Mechanistic insights into electrochemical nitrogen reduction reaction on vanadium nitride nanoparticles. *J Am Chem Soc* 2018;140:13387-91. DOI
8. Gao Y, Zhuo H, Cao Y, et al. A theoretical study of electrocatalytic ammonia synthesis on single metal atom/MXene. *Chinese J Catal* 2019;40:152-9. DOI
9. Wu J, Li JH, Yu YX. Single Nb or W atom-embedded BP monolayers as highly selective and stable electrocatalysts for nitrogen fixation with low-onset potentials. *ACS Appl Mater Interfaces* 2021;13:10026-36. DOI PubMed
10. Du P, Huang Y, Zhu G, et al. Nitrogen reduction reaction on single cluster catalysts of defective PC₆-trimeric or tetrameric transition metal. *Phys Chem Chem Phys* 2022;24:2219-26. DOI PubMed
11. Andersen SZ, Čolić V, Yang S, et al. A rigorous electrochemical ammonia synthesis protocol with quantitative isotope measurements. *Nature* 2019;570:504-8. DOI
12. Zhang L, Meng Y, Shen H, et al. High-efficiency photocatalytic ammonia synthesis by facet orientation-supported heterojunction Cu₂O@BiOCl[100] boosted by double built-in electric fields. *Inorg Chem* 2022;61:6045-55. DOI
13. Li L, Tang C, Yao D, Zheng Y, Qiao SZ. Electrochemical nitrogen reduction: identification and elimination of contamination in electrolyte. *ACS Energy Lett* 2019;4:2111-6. DOI
14. Hao YC, Guo Y, Chen LW, et al. Promoting nitrogen electroreduction to ammonia with bismuth nanocrystals and potassium cations in water. *Nat Catal* 2019;2:448-56. DOI
15. Singh AR, Rohr BA, Statt MJ, Schwalbe JA, Cargnello M, Nørskov JK. Strategies toward selective electrochemical ammonia synthesis. *ACS Catal* 2019;9:8316-24. DOI
16. Martín AJ, Shinagawa T, Pérez-ramírez J. Electrocatalytic reduction of nitrogen: from haber-bosch to ammonia artificial leaf. *Chem* 2019;5:263-83. DOI
17. Han B, Meng H, Li F, Zhao J. Fe₃ cluster anchored on the C₂N monolayer for efficient electrochemical nitrogen fixation. *Catalysts* 2020;10:974. DOI
18. Yu L, Li F. Pt₂ dimer anchored vertically in defective BN monolayer as an efficient catalyst for N₂ reduction: a DFT study. *Catalysts* 2022;12:1387. DOI
19. Geng Z, Liu Y, Kong X, et al. Achieving a record-high yield rate of 120.9 μg_{NH₃}·mg_{cat}⁻¹·h⁻¹ for N₂ electrochemical reduction over Ru single-atom catalysts. *Adv Mater* 2018;30:1803498. DOI
20. Tao H, Choi C, Ding LX, et al. Nitrogen fixation by Ru single-atom electrocatalytic reduction. *Chem* 2019;5:204-14. DOI
21. Han Z, Huang S, Zhang J, et al. Single Ru-N₄ site-embedded porous carbons for electrocatalytic nitrogen reduction. *ACS Appl Mater Interfaces* 2023;15:13025-32. DOI
22. Nørskov JK, Bligaard T, Hvolbaek B, Abild-Pedersen F, Chorkendorff I, Christensen CH. The nature of the active site in heterogeneous metal catalysis. *Chem Soc Rev* 2008;37:2163-71. DOI PubMed
23. Azofra LM, Li N, MacFarlane DR, Sun C. Promising prospects for 2D d²-d⁴ M₃C₂ transition metal carbides (MXenes) in N₂ capture and conversion into ammonia. *Energy Environ Sci* 2016;9:2545-9. DOI
24. Choi C, Back S, Kim NY, Lim J, Kim YH, Jung Y. Suppression of hydrogen evolution reaction in electrochemical N₂ reduction using single-atom catalysts: a computational guideline. *ACS Catal* 2018;8:7517-25. DOI
25. Skúlason E, Bligaard T, Gudmundsdóttir S, et al. A theoretical evaluation of possible transition metal electro-catalysts for N₂ reduction. *Phys Chem Chem Phys* 2012;14:1235-45. DOI
26. Liu L, Corma A. Metal catalysts for heterogeneous catalysis: from single atoms to nanoclusters and nanoparticles. *Chem Rev* 2018;118:4981-5079. DOI PubMed PMC

27. Su P, Pei W, Wang X, et al. Exceptional electrochemical HER performance with enhanced electron transfer between Ru nanoparticles and single atoms dispersed on a carbon substrate. *Angew Chem Int Ed Engl* 2021;60:16044-50. DOI
28. Yang XF, Wang A, Qiao B, Li J, Liu J, Zhang T. Single-atom catalysts: a new frontier in heterogeneous catalysis. *Acc Chem Res* 2013;46:1740-8. DOI
29. Lv X, Wei W, Wang H, Huang B, Dai Y. Holey graphitic carbon nitride (g-CN) supported bifunctional single atom electrocatalysts for highly efficient overall water splitting. *Appl Catal B Environ* 2020;264:118521. DOI
30. Zhao J, Chen Z. Single Mo atom supported on defective boron nitride monolayer as an efficient electrocatalyst for nitrogen fixation: a computational study. *J Am Chem Soc* 2017;139:12480-7. DOI
31. Zhao J, Zhao J, Cai Q. Single transition metal atom embedded into a MoS₂ nanosheet as a promising catalyst for electrochemical ammonia synthesis. *Phys Chem Chem Phys* 2018;20:9248-55. DOI
32. Chen Z, Zhao J, Cabrera CR, Chen Z. Computational screening of efficient single-atom catalysts based on graphitic carbon nitride (g-C₃N₄) for nitrogen electroreduction. *Small Methods* 2019;3:1800368. DOI
33. He T, Matta SK, Will G, Du A. Transition-metal single atoms anchored on graphdiyne as high-efficiency electrocatalysts for water splitting and oxygen reduction. *Small Methods* 2019;3:1800419. DOI
34. Liu Y, Xu Q, Fan X, et al. Electrochemical reduction of N₂ to ammonia on Co single atom embedded N-doped porous carbon under ambient conditions. *J Mater Chem A* 2019;7:26358-63. DOI
35. Wang S, Wei W, Lv X, Huang B, Dai Y. W supported on g-CN manifests high activity and selectivity for N₂ electroreduction to NH₃. *J Mater Chem A* 2020;8:1378-85. DOI
36. Yu X, Pei W, Xu W, Zhao Y, Su Y, Zhao J. Core-packing-related vibrational properties of thiol-protected gold nanoclusters and their excited-state behavior. *Inorg Chem* 2023;62:20450-7. DOI
37. Zhao J, Du Q, Zhou S, Kumar V. Endohedrally doped cage clusters. *Chem Rev* 2020;120:9021-163. DOI PubMed
38. Yu X, Sun Y, Xu W, et al. Tuning photoelectron dynamic behavior of thiolate-protected MAu₂₄ nanoclusters via heteroatom substitution. *Nanoscale Horiz* 2022;7:1192-200. DOI
39. Yan H, Lin Y, Wu H, et al. Bottom-up precise synthesis of stable platinum dimers on graphene. *Nat Commun* 2017;8:1070. DOI PubMed PMC
40. Li G, Li Y, Liu H, Guo Y, Li Y, Zhu D. Architecture of graphdiyne nanoscale films. *Chem Commun* 2010;46:3256-8. DOI
41. Tian S, Fu Q, Chen W, et al. Carbon nitride supported Fe₂ cluster catalysts with superior performance for alkene epoxidation. *Nat Commun* 2018;9:2353. DOI PubMed PMC
42. Ji S, Chen Y, Fu Q, et al. Confined pyrolysis within metal-organic frameworks to form uniform Ru₃ clusters for efficient oxidation of alcohols. *J Am Chem Soc* 2017;139:9795-8. DOI
43. Pei W, Hou L, Yu X, et al. Graphitic carbon nitride supported trimeric metal clusters as electrocatalysts for N₂ reduction reaction. *J Catal* 2024;429:115232. DOI
44. Li Y, Zhang Q, Li C, et al. Atomically dispersed metal dimer species with selective catalytic activity for nitrogen electrochemical reduction. *J Mater Chem A* 2019;7:22242-7. DOI
45. Li H, Zhao Z, Cai Q, Yin L, Zhao J. Nitrogen electroreduction performance of transition metal dimers embedded into N-doped graphene: a theoretical prediction. *J Mater Chem A* 2020;8:4533-43. DOI
46. Zheng G, Li L, Tian Z, Zhang X, Chen L. Heterogeneous single-cluster catalysts (Mn₃, Fe₃, Co₃, and Mo₃) supported on nitrogen-doped graphene for robust electrochemical nitrogen reduction. *J Energy Chem* 2021;54:612-9. DOI
47. Cui C, Zhang H, Luo Z. Nitrogen reduction reaction on small iron clusters supported by N-doped graphene: a theoretical study of the atomically precise active-site mechanism. *Nano Res* 2020;13:2280-8. DOI
48. Li L, Xu L. Design of a graphene nitrene two-dimensional catalyst providing a well-defined site accommodating up to three metals, with application to N₂ reduction electrocatalysis. *Chem Commun* 2020;56:8960-3. DOI
49. Kresse G, Hafner J. Ab initio molecular dynamics for liquid metals. *Phys Rev B Condens Matter* 1993;47:558-61. DOI PubMed
50. Kresse G, Hafner J. Ab initio molecular-dynamics simulation of the liquid-metal-amorphous-semiconductor transition in germanium. *Phys Rev B Condens Matter* 1994;49:14251-69. DOI PubMed
51. Kresse G, Joubert D. From ultrasoft pseudopotentials to the projector augmented-wave method. *Phys Rev B* 1999;59:1758. DOI
52. Blöchl PE. Projector augmented-wave method. *Phys Rev B Condens Matter* 1994;50:17953-79. DOI PubMed
53. Perdew JP, Burke K, Ernzerhof M. Generalized gradient approximation made simple. *Phys Rev Lett* 1996;77:3865. DOI PubMed
54. Tian J, Hou L, Xia W, et al. Solar driven CO₂ hydrogenation to HCOOH on (TiO₂)_n (n = 1-6) atomic clusters. *Phys Chem Chem Phys* 2023;25:28533-40. DOI
55. Grimme S, Antony J, Ehrlich S, Krieg H. A consistent and accurate *ab initio* parametrization of density functional dispersion correction (DFT-D) for the 94 elements H-Pu. *J Chem Phys* 2010;132:154104. DOI PubMed
56. Grimme S, Ehrlich S, Goerigk L. Effect of the damping function in dispersion corrected density functional theory. *J Comput Chem* 2011;32:1456-65. DOI PubMed
57. Monkhorst HJ, Pack JD. Special points for Brillouin-zone integrations. *Phys Rev B* 1976;13:5188. DOI
58. Peterson AA, Abild-Pedersen F, Studt F, Rossmeisl J, Nørskov JK. How copper catalyzes the electroreduction of carbon dioxide into hydrocarbon fuels. *Energy Environ Sci* 2010;3:1311-5. DOI
59. Peterson AA, Nørskov JK. Activity descriptors for CO₂ electroreduction to methane on transition-metal catalysts. *J Phys Chem Lett* 2012;3:251-8. DOI

60. Nørskov JK, Rossmeisl J, Logadottir A, et al. Origin of the overpotential for oxygen reduction at a fuel-cell cathode. *J Phys Chem B* 2004;108:17886-92. DOI
61. Lv X, Wei W, Huang B, Dai Y, Frauenheim T. High-throughput screening of synergistic transition metal dual-atom catalysts for efficient nitrogen fixation. *Nano Lett* 2021;21:1871-8. DOI
62. Zhou Y, Wang J, Liang L, et al. Unraveling the size-dependent effect of Ru-based catalysts on ammonia synthesis at mild conditions. *J Catal* 2021;404:501-11. DOI
63. Wang S, Shi L, Bai X, Li Q, Ling C, Wang J. Highly efficient photo-/electrocatalytic reduction of nitrogen into ammonia by dual-metal sites. *ACS Cent Sci* 2020;6:1762-71. DOI PubMed PMC
64. Ling C, Niu X, Li Q, Du A, Wang J. Metal-free single atom catalyst for N₂ fixation driven by visible light. *J Am Chem Soc* 2018;140:14161-8. DOI
65. Hu R, Li Y, Zeng Q, Wang F, Shang J. Bimetallic pairs supported on graphene as efficient electrocatalysts for nitrogen fixation: search for the optimal coordination atoms. *ChemSusChem* 2020;13:3636-44. DOI PubMed
66. Pei W, Zhou S, Zhao J, Du Y, Dou SX. Optimization of photocarrier dynamics and activity in phosphorene with intrinsic defects for nitrogen fixation. *J Mater Chem A* 2020;8:20570-80. DOI
67. Janesko BG. Replacing hybrid density functional theory: motivation and recent advances. *Chem Soc Rev* 2021;50:8470-95. DOI PubMed
68. Shinde R, Yamijala SSRKC, Wong BM. Improved band gaps and structural properties from Wannier-Fermi-Löwdin self-interaction corrections for periodic systems. *J Phys Condens Matter* 2021;33:115501. DOI PubMed
69. Back S, Lim J, Kim NY, Kim YH, Jung Y. Single-atom catalysts for CO₂ electroreduction with significant activity and selectivity improvements. *Chem Sci* 2017;8:1090-6. DOI PubMed PMC
70. Li H, Pei W, Yang X, Zhou S, Zhao J. Pt overlayer for direct oxidation of CH₄ to CH₃OH. *Chinese Chem Lett* 2023;34:108292. DOI
71. Zhou S, Pei W, Du Q, Zhao J. Foreign atom encapsulated Au₁₂ golden cages for catalysis of CO oxidation. *Phys Chem Chem Phys* 2019;21:10587-93. DOI
72. Pei W, She J, Yu X, Zhou S, Zhao J. Atomically precise gold nanoclusters for CO oxidation: balancing activity and stability by ligand shedding. *J Phys D Appl Phys* 2023;56:445304. DOI
73. Han B, Li F. Regulating the electrocatalytic performance for nitrogen reduction reaction by tuning the N contents in Fe₃@N_xC_{20-x} (x = 0~4): a DFT exploration. *J Mater Inf* 2023;3:24. DOI
74. Gu YT, Gu YM, Tao Q, Wang X, Zhu Q, Ma J. Machine learning for prediction of CO₂/N₂/H₂O selective adsorption and separation in metal-zeolites. *J Mater Inf* 2023;3:19. DOI
75. Hu Y, Chen J, Wei Z, He Q, Zhao Y. Recent advances and applications of machine learning in electrocatalysis. *J Mater Inf* 2023;3:18. DOI
76. Sun Y, Pei W, Xie M, et al. Excitonic Au₄Ru₂(PPh₃)₂(SC₂H₄Ph)₈ cluster for light-driven dinitrogen fixation. *Chem Sci* 2020;11:2440-7. DOI PubMed PMC
77. Zhou S, Pei W, Zhao Y, Yang X, Liu N, Zhao J. Low-dimensional non-metal catalysts: principles for regulating p-orbital-dominated reactivity. *npj Comput Mater* 2021;7:186. DOI